International Journal of Bifurcation and Chaos, Vol. 5, No. 1 (1995) 133–144

CHAOTIC MIXING IN RIGID, PERFECTLY PLASTIC MATERIAL

B. F. FEENY
Department of Mechanical Engineering, Michigan State University, East Lansing, MI 48824, USA

F. C. MOON
Sibley School of Mechanical and Aerospace Engineering, Cornell University, Ithaca, NY 14853, USA

P. Y. CHEN
Chung-Shan Institute of Science and Technology, Tauyuan, Taiwan, ROC

S. MUKHERJEE
Theoretical and Applied Mechanics, Cornell University, Ithaca, NY 14853, USA

Received July 2, 1991; Revised July 5, 1994

An example of Lagrangian chaos or mixing in a solid material is presented here. The mixing due to cyclic torques of rigid, perfectly plastic sheet is simulated. The plastic flow results in an area-preserving map. Results are displayed as Poincaré maps, the stretching and folding of an initial line of material points, the mixing of initial regions, and the eigenvalues about initial points during one mixing cycle. The Poincaré sections show ite. .tes of sets of points after each cycle of deformation. The mixing diagrams provide evidence for horseshoe-like processes in the dynamics. Single-cycle eigenvalues exhibit self similarity in the spatial structure.

1. Introduction

The problem of mixing, stirring, or advection has been studied for fluids under a Stokes flow, which is a creeping kinematic flow with no inertial and dynamical effects [Aref, 1984, 1986; Chaiken *et al.*, 1989; Ottino, 1989a; Franjione *et al.*, 1989; Ling, 1993a], and has been shown to be a practical application of ideas of chaos. Through such studies, efficient methods have been developed for enhancing chemical reactions and making polymers (see also Ling [1993b] and the conference proceedings edited by Acrivos [1991]). The study of mixing may also provide insight to geothermal processes, such as the flow of magma [Ottino, 1989b].

In this paper, we examine the phenomenon of Lagrangian chaos in the mixing of rigid, perfectly plastic materials. Mixing of plastic materials has long been done by ceramic artists, producing swirling patterns on pottery. There may be technical applications in forging processes and other deformation-based forming processes. Furthermore, studies of plastic materials may be applied to viscoelastic materials when the deformation rate is very slow.

In the case examined here, the flow of rigid perfectly plastic material is solvable under some simplifying assumptions. This yields a simple map, which provides a scarce opportunity for analysis of mixing flows. Our exploratory goal is to produce mixing diagrams, Poincaré sections, and to quantify stretching. Stretching can be useful in studying mixing models, as done by Ottino *et al.* [1994] by means

of horseshoe maps. The mixing diagrams involve the use of color coding to show how four quadrants of the two-dimensional material slab deform under several iterations of the mixing cycle. The example in this paper is a variation of the "blinking vortex" models studied by Aref [1984] and Ottino [1989b], but with a logarithmic flow field appropriate to plastic materials replacing the vortex flow field.

A torque is applied about a point A in a sheet of rigid, perfectly plastic material through a body-force distribution F_θ (per unit volume) in the tangential direction in terms of polar coordinates (r, θ) centered at A:

$$F_\theta = -\frac{2K}{r}. \tag{1}$$

Here, K is a constant. The body force (1) produces a uniform shearing stress distribution,

$$\tau_{r\theta} = K, \tag{2}$$

which satisfies the equilibrium equations for a differential element [Timoshenko & Goodier, 1970]:

$$\frac{d\tau_{r\theta}}{dr} + \frac{2\tau_{r\theta}}{r} + F_\theta = 0. \tag{3}$$

We adopt the rigid, perfectly plastic model, which is an idealized model of plastic flow in a material (see, e.g., Mendelson [1968]). For values of shear stress less than τ_0, the material remains rigid.

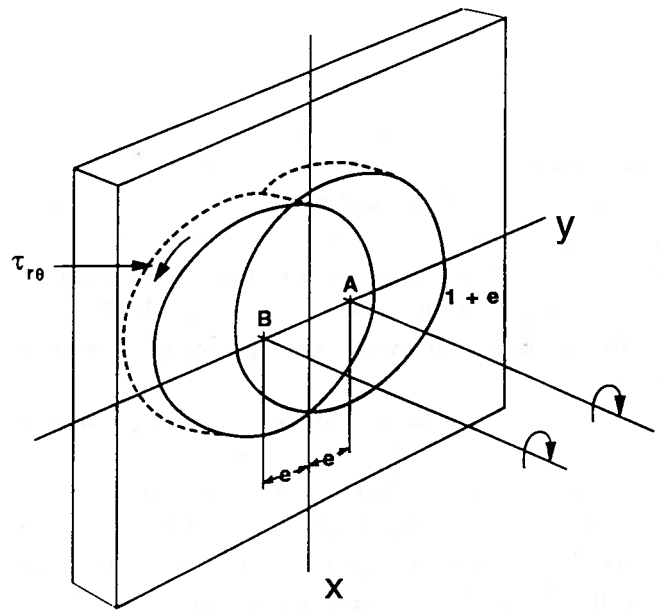

Fig. 1. Sketch of plastic sheet showing the two zones of deformation centered at the points A and B, located at (x, y) coordinates $(0, e)$ and $(0, -e)$, respectively.

However, the material yields and flows when $K = \tau_0$, where τ_0 is the yield stress of the material in shear.

Our mixing plan is to apply a torque at a point A on the plastic sheet, and allow material to flow for a certain amount of time. We then apply the torque at another position B, and allow material to flow for the same amount of time. The torque is to be alternated between positions A and B (Fig. 1). The patterns of flow are then to be observed as in the blinking vortex model [Ottino, 1989a].

2. Development of the Dynamical Equations

Given the body-torque distribution (1) on an infinite plane of plastic material, and assuming that there are no inertial effects, the deformation of a material point can be written in terms of a simple function. In polar coordinates, the shear strain rate can be expressed as

$$\dot{\gamma}_{r\theta} = \frac{\partial u}{r\partial\theta} + \frac{\partial v}{\partial r} - \frac{v}{r}, \tag{4}$$

where u is the deformation rate in the radial direction, and v is the deformation rate in the tangential direction [Timoshenko & Goodier, 1970]. In the theory of plasticity, the strain rate is related to the stress by a flow rule when the stress reaches the yield value τ_0;

$$\dot{\gamma}_{r\theta} = \alpha\tau_{r\theta} = \alpha\tau_0, \tag{5}$$

where α is a proportionality constant. If we assume that the deformation is tangential during each half cycle, then Eq. (4) becomes

$$\frac{dv}{dr} - \frac{v}{r} = \alpha\tau_o. \tag{6}$$

The general solution to this equation is of the form

$$v = r(\alpha\tau_o \ln r + C), \tag{7}$$

where C is a constant of integration.

We restrict the applied body torque to a circular disc of radius $r = a$ (see Fig. 1). Thus, we impose boundary conditions $v(a) = 0$, and obtain a tangential deformation rate

$$v(r) = \alpha\tau_0 r \ln\frac{r}{a}. \tag{8}$$

In terms of rotation, the angular deformation is $\theta = t\alpha\tau_0 \ln\frac{r}{a}$, where t is the time for which the torque

is applied. Rescaling distance and time such that $\hat{r} = r/a$ and $\tau = \lambda\tau_0 t$, and dropping the hat on $\hat{r}$, the expression for angular deformation is

$$\theta = \tau \ln r\,, \tag{9}$$

valid for $0 < r \leq 1$. The only parameter is the nondimensional time τ of the applied torque. That is, for any material parameters, and a yielding torque, the time of the torque can be chosen to obtain a desired angular displacement. (Increasing the radius of the body torque causes an increase in the radius of the deformation zone, which is rescaled to $r = 1$ in the nondimensionalization.)

In the numerical simulation, a torque centered at a point A for a time τ deforms material within a radius of $r = 1$. Then the same deformation history is applied at a point B for a time τ, located a distance $2e$ from point A, and deforms material within a radius of 1. Alternating the deformations about points A and then B defines a cycle. The Cartesian coordinates of A and B are defined as $(0, e)$ and $(0, -e)$, respectively. Initial conditions (x, y) are translated into polar coordinates (r_A, θ_A) centered at A. The material point evolves according to (9) such that

$$\begin{aligned} \theta_A^{n+1} &= \theta_A^n + \tau \ln r^n\,, \\ r_A^{n+1} &= r_A^n\,, \end{aligned} \tag{10}$$

where the superscripts denote the cycle count, not a power. The values of r_A^{n+1} and θ_A^{n+1} are converted to polar coordinates (r_B, θ_B) centered at B. During the torque at B, the material deforms and we have

$$\begin{aligned} \theta_B^{m+1} &= \theta_B^m + \tau \ln r^m\,, \\ r_B^{m+1} &= r_B^m\,, \end{aligned} \tag{11}$$

completing a cycle of motion. The values of r_B and θ_B are converted to r_A and θ_A and the process is iterated.

The eccentricity e of points A and B introduces a second control parameter in addition to the torque duration τ. The study could be explored further by varying the sequence of torques, which defines a cycle, as done by Franjione *et al.* [1989].

3. Area Preservation

The plastic flow is area preserving, as can be guessed by the Hamiltonian-looking Poincaré maps of Figs. 2. This can be shown by translating Eqs. (10) and (11) into Cartesian coordinates. To do so, we substitute Eqs. (10) or (11) into

$$\begin{aligned} x_{A,B}^{n+1} &= r^{n+1} \cos\theta^{n+1}\,, \\ y_{A,B}^{n+1} &= r^{n+1} \sin\theta^{n+1}\,, \end{aligned}$$

where $x_{A,B}$ and $y_{A,B}$ are the Cartesian coordinates centered at A or B. After some algebra,

$$\begin{aligned} x_{A,B}^{n+1} &= x_{A,B}^n \cos(\tau \ln r^n) \\ &\quad - y_{A,B}^n \sin(\tau \ln r^n)\,, \\ x_{A,B}^{n+1} &= y_{A,B}^n \cos(\tau \ln r^n) \\ &\quad + x_{A,B}^n \sin(\tau \ln r^n)\,. \end{aligned} \tag{12}$$

These equations can be expressed as a vector equation $\mathbf{z}_{A,B}^{n+1} = \mathbf{F}(\mathbf{z}_{A,B}^n)$, where $\mathbf{z} = [x, y]^T$. In a given cycle, some material points deform via $\mathbf{F}$ centered at A or B only. Others deform through a composition of $\mathbf{F}$ centered at A and $\mathbf{F}$ centered at B. A full cycle of torque will be represented by $\mathbf{z}_{n+1} = \mathbf{G}(\mathbf{z}_n)$. For each half cycle, the Jacobian $D\mathbf{F}$ is given by

$$D\mathbf{F} = \begin{bmatrix} \left(1 - \dfrac{xy}{r^2}\tau\right)\cos\psi - \dfrac{x^2}{r^2}\tau\sin\psi & -\dfrac{y^2}{r^2}\tau\cos\psi - \left(1 + \dfrac{xy}{r^2}\tau\right)\sin\psi \\ \dfrac{x^2}{r^2}\tau\cos\psi + \left(1 - \dfrac{xy}{r^2}\tau\right)\sin\psi & \left(1 + \dfrac{xy}{r^2}\tau\right)\cos\psi - \dfrac{y^2}{r^2}\tau\sin\psi \end{bmatrix} \tag{13}$$

where $\psi = \tau \log r$ and $r = \sqrt{x^2 + y^2}$. Then, $\det D\mathbf{F} = 1$ for all x and y, making the map area preserving. The whole cycle, being a composition of area-preserving maps, is also area preserving.

The eigenvalues of $D\mathbf{F}$ are $\gamma = (T \pm \sqrt{T^2 - 4})/2$, where $T = \text{trace } D\mathbf{F} = 2\cos\psi - \tau\sin\psi$. Thus the torque time τ has a direct effect on the achievable eigenvalues. As r varies, T oscillates with a

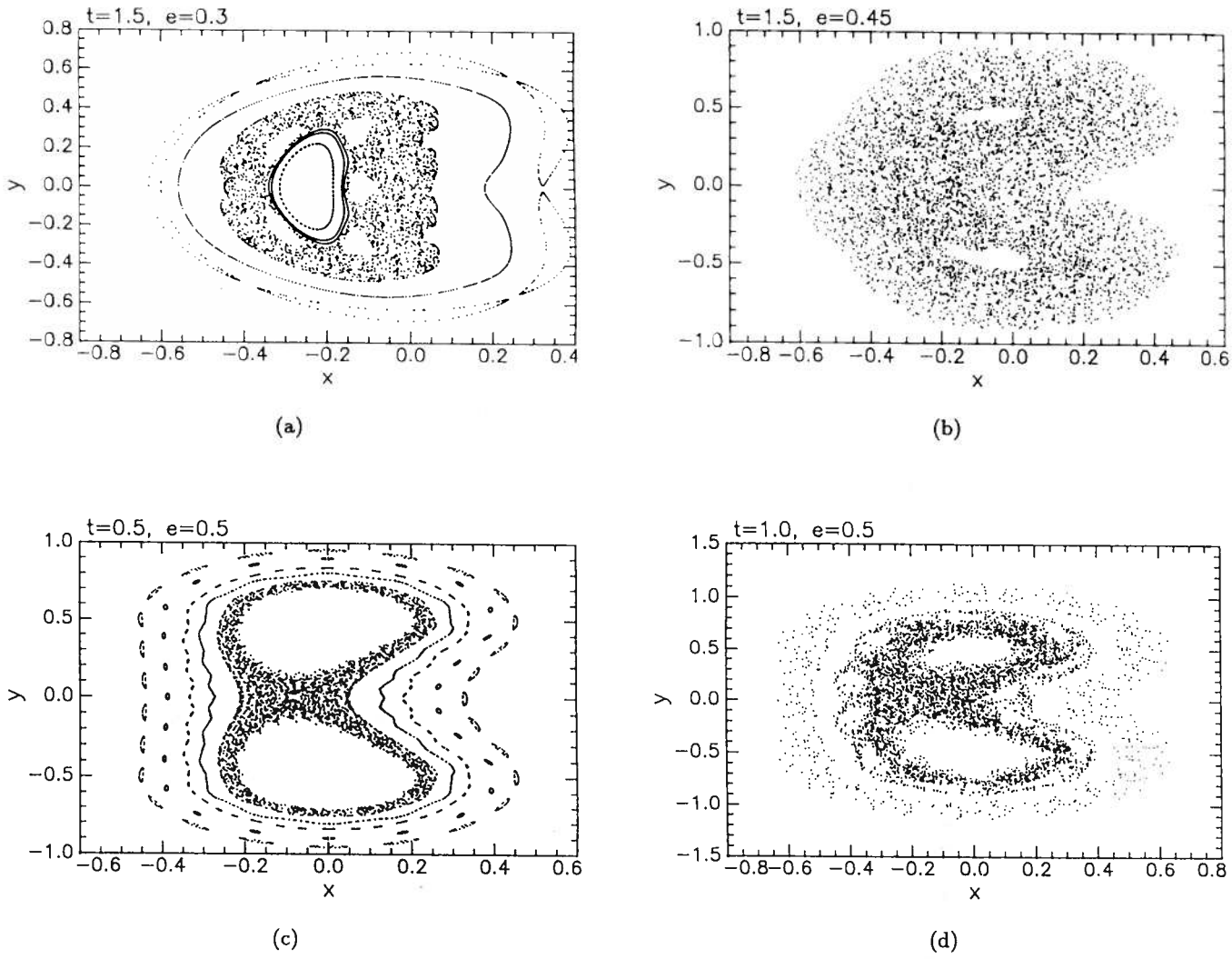

Fig. 2. Poincaré maps for the mixing of plastic material for various eccentricities and torque durations: (a) $e = 0.3$, $\tau = 1.5$, (b) $e = 0.45$, $\tau = 1.5$, (c) $e = 0.5$, $\tau = 0.5$, and (d) $e = 0.5$, $\tau = 1.0$. There are ten initial conditions, and each is iterated 500 times.

wavelength proportional to $1/|\log(r)|$. This wavelength is very small for small r.

4. Numerical Results

The similation parameters are τ and e. We present the results in four ways: Poincaré maps, the stretching and folding of an initial line of material points, the mixing of initial regions, and the spatial distribution of eigenvalues during one cycle.

Poincaré maps are shown in Figs. 2, showing the effects of varying either parameter. These maps show the stroboscopic motion of several different initial points in the plane at the end of each of the deformation cycles. Closed orbits show quasiperiodic dynamics. Seemingly random collections of points give evidence for Hamiltonian chaos or stochasticity. Stochasticity increases with increasing τ. There is a maximum of stochasticity with respect to eccentricity. If $e = 0$ (the circles of deformation are identical), and similarly if $e \geq 1$ (the circles of deformation are disjoint), then there is no stochasticity. The data in Fig. 2 show the result of several hundred iterations. In contrast, Figs. 3–7 (discussed below) show the dynamics after only a few cycles.

Deformation of an initial line element is shown in Fig. 3 for various parameter settings and at various cycles. Some portions of an initial line stretch much more than other segments. It is likely that the high stretching corresponds to high

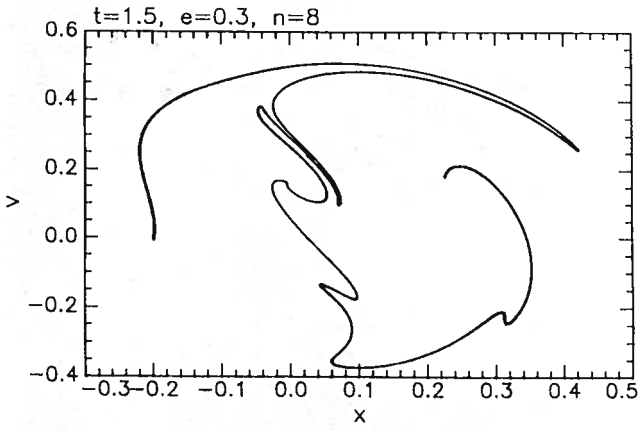

(a)

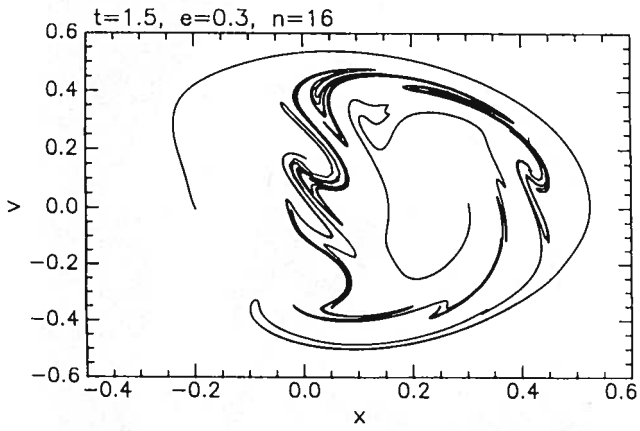

(b)

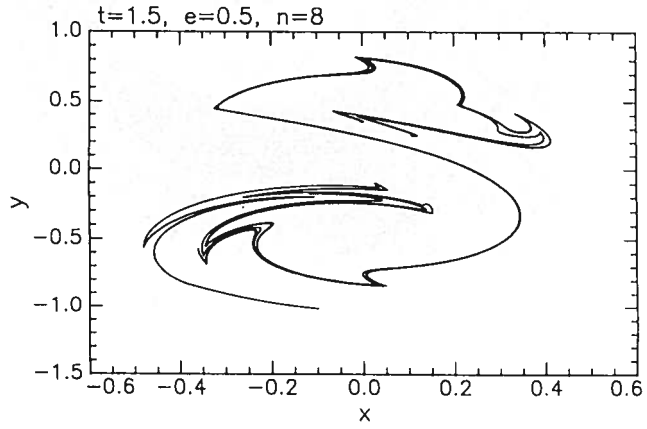

(c)

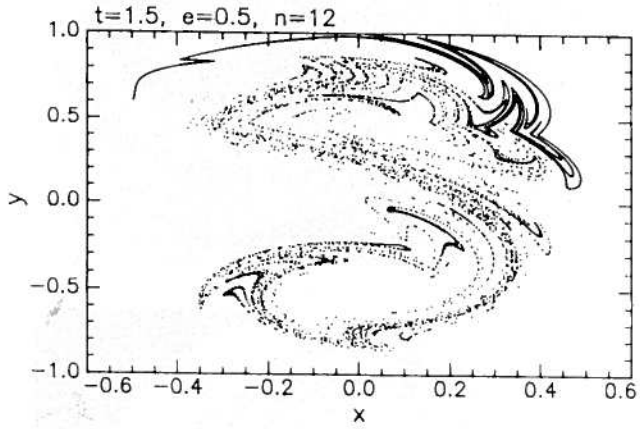

(d)

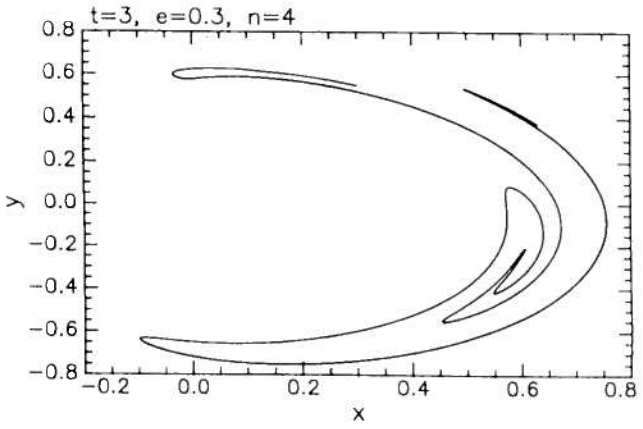

(e)

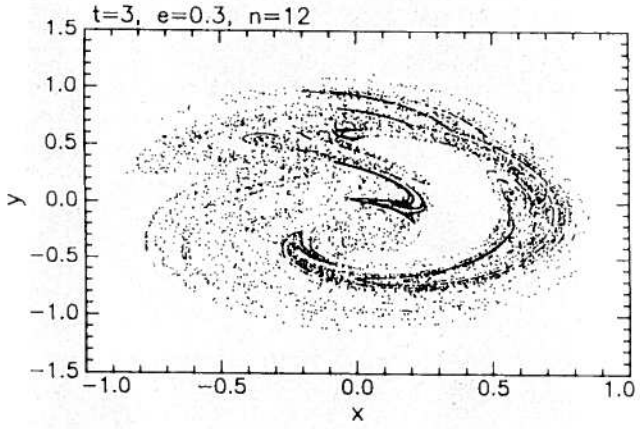

(f)

Fig. 3. The mixing of an initial line element for various eccentricities and torque durations: (a) $e = 0.3$, $\tau = 1.5$, $n = 8$, (b) $e = 0.3$, $\tau = 1.5$, $n = 16$, (c) $e = 0.5$, $\tau = 1.5$, $n = 8$, (d) $e = 0.5$, $\tau = 1.5$, $n = 12$, (e) $e = 0.3$, $\tau = 3.0$, $n = 4$, and (f) $e = 0.3$, $\tau = 3.0$, $n = 12$.

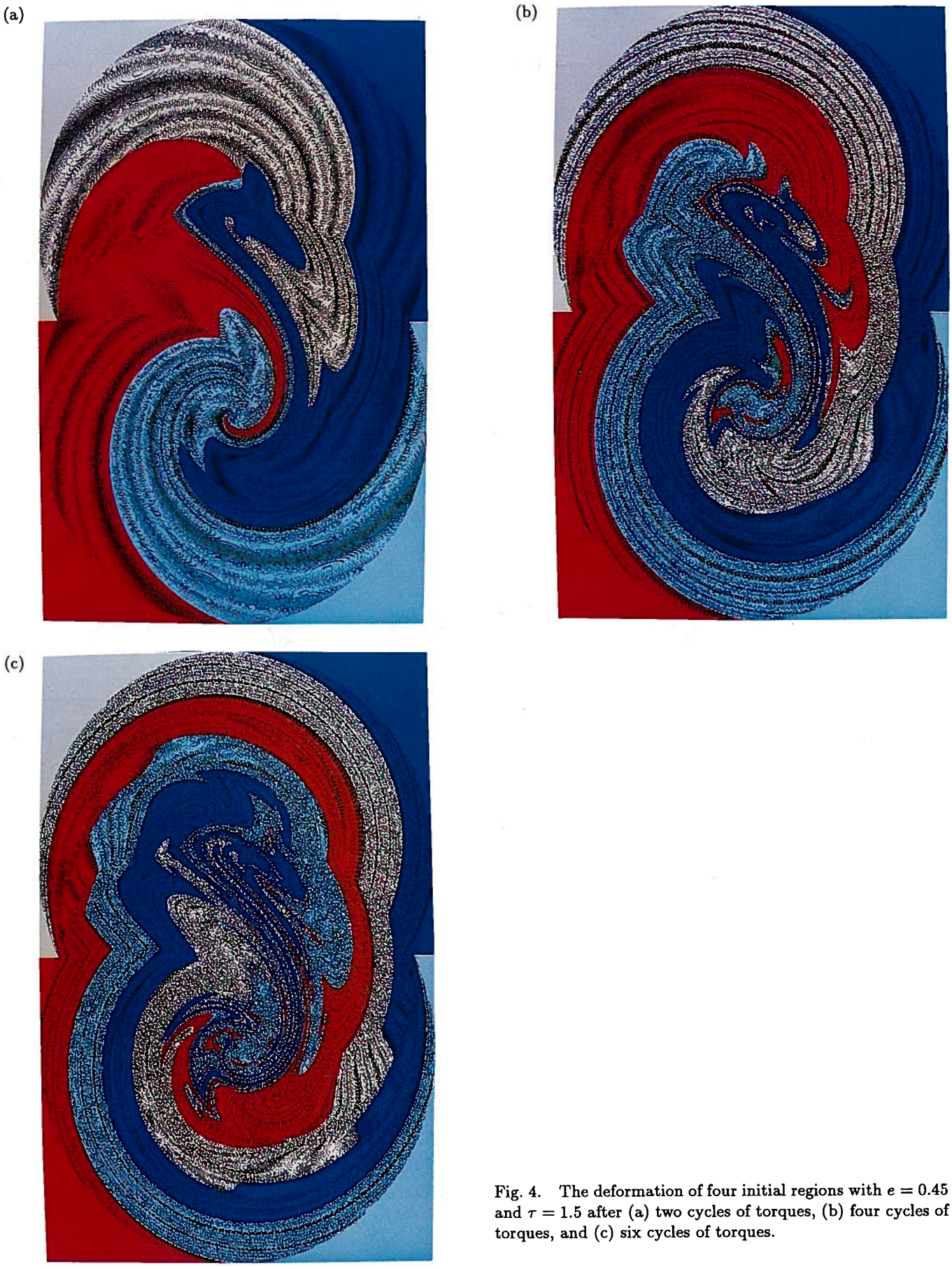

Fig. 4. The deformation of four initial regions with $e = 0.45$ and $\tau = 1.5$ after (a) two cycles of torques, (b) four cycles of torques, and (c) six cycles of torques.

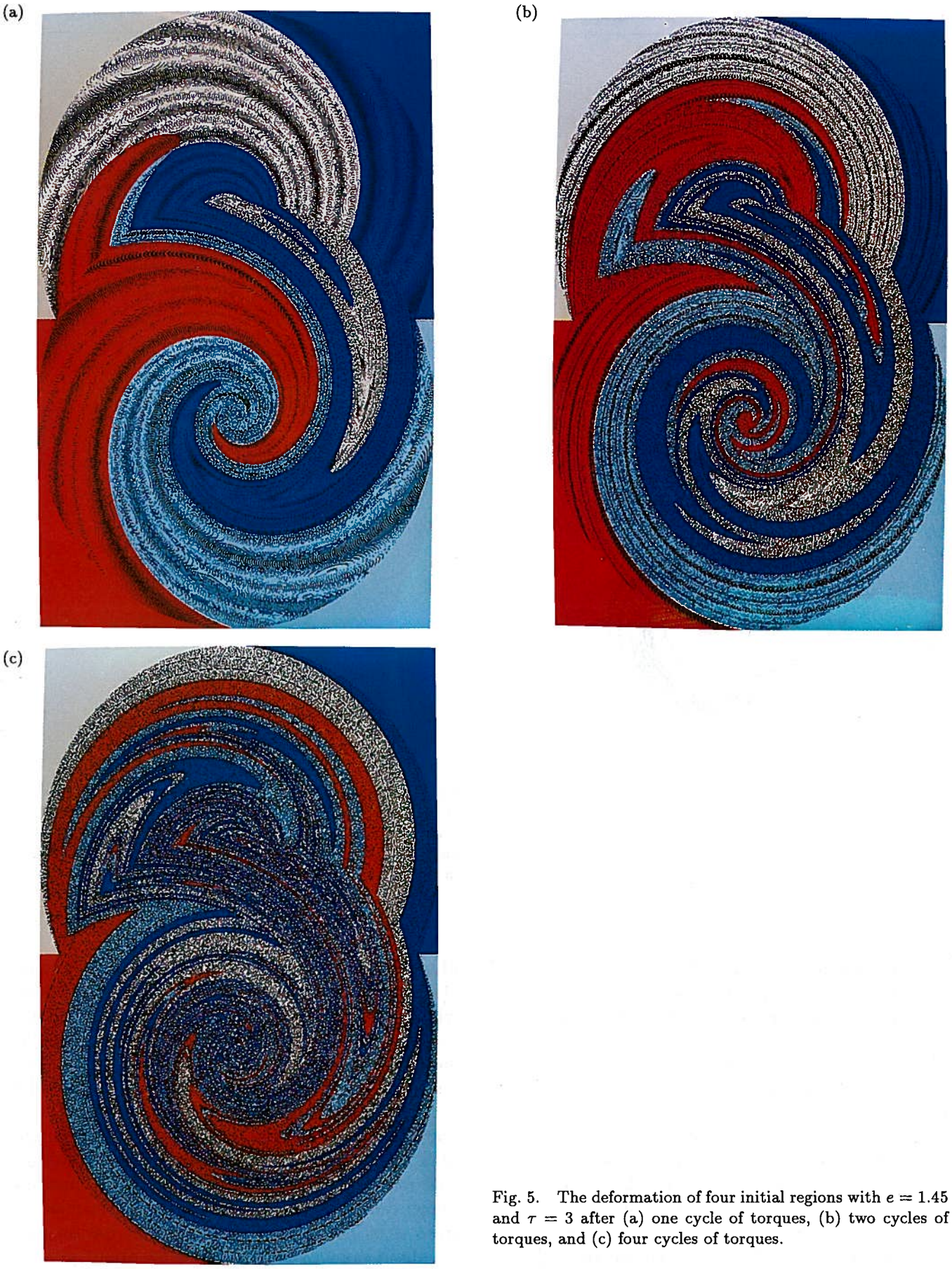

Fig. 5. The deformation of four initial regions with $e = 1.45$ and $\tau = 3$ after (a) one cycle of torques, (b) two cycles of torques, and (c) four cycles of torques.

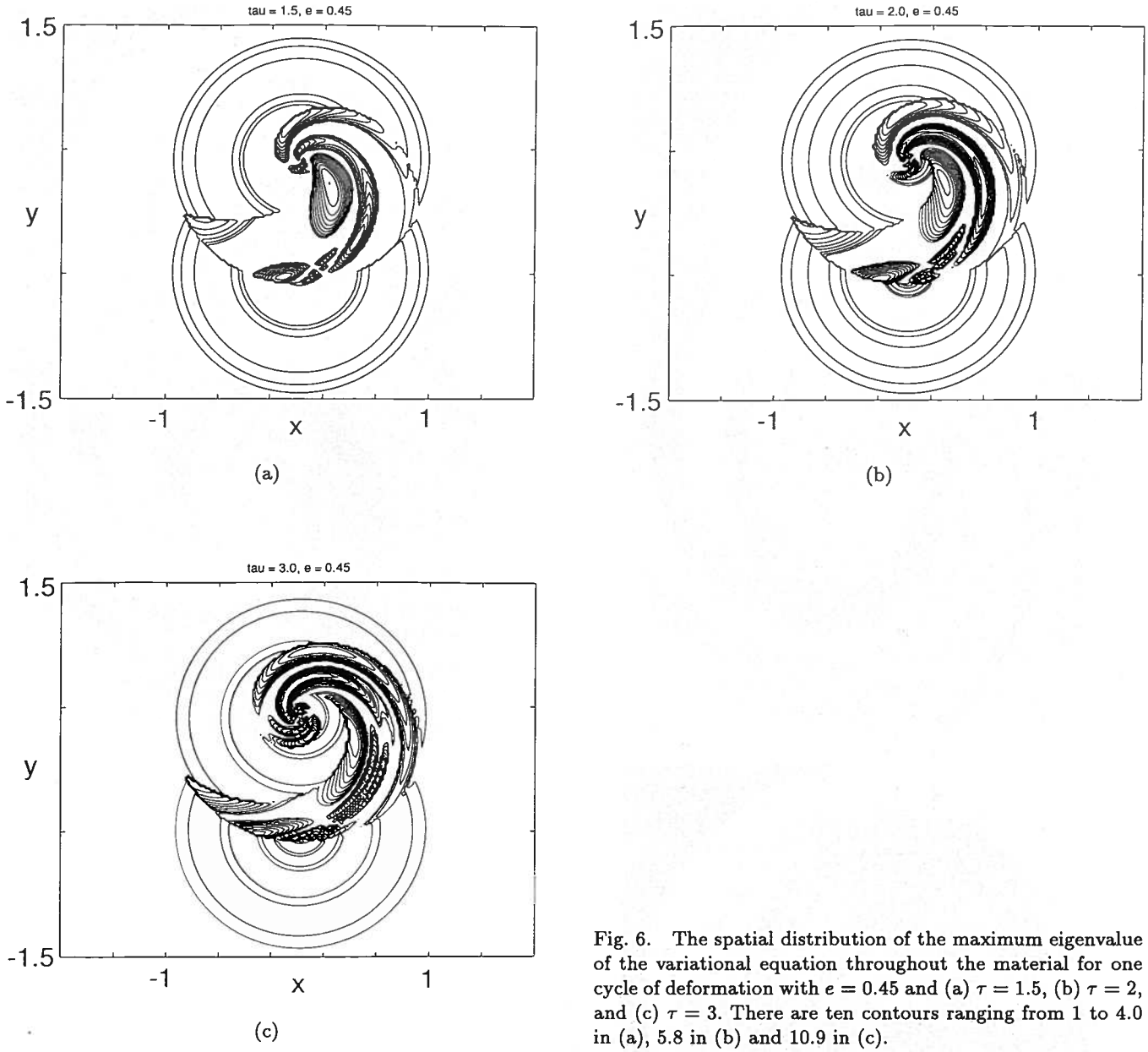

Fig. 6. The spatial distribution of the maximum eigenvalue of the variational equation throughout the material for one cycle of deformation with $e = 0.45$ and (a) $\tau = 1.5$, (b) $\tau = 2$, and (c) $\tau = 3$. There are ten contours ranging from 1 to 4.0 in (a), 5.8 in (b) and 10.9 in (c).

stochasticity in the Poincaré maps. The folding of the line elements under the map gives some evidence for the horseshoe-producing nature of the map.

Deformation of the four quadrants of material is shown in Figs. 4 and 5. In the simulation, each initial point has an associated color, determined by its quadrant. After a few iterations, the material point is relocated, and plotted in its color. Under careful observation, the material point which started at the origin (the four-corners point) can be detected.

Next, we compute the eigenvalues of the variational map about a material point during one cycle. Material points which merely deform through one of the half cycles are associated with the Jacobian (13) evaluated at the initial point. Material points which deform through both parts of the cycle have a Jacobian consisting of a composition of half-cycle Jacobians coupled with a rotation matrix $\mathbf{R}_\phi$. The half-cycle Jacobians $D\mathbf{F}$ are evaluated at the points (x_A, y_A) (referring to a deformation centered at A) and at (x_B, y_B) (referring to a deformation centered at B). $\mathbf{R}_\phi$ represents the change in orientation of this material point, with respect to the instantaneous center of torque, as the torque is relocated from A to B. Such a material point has an angle θ_A about point A and an angle θ_B about point B.

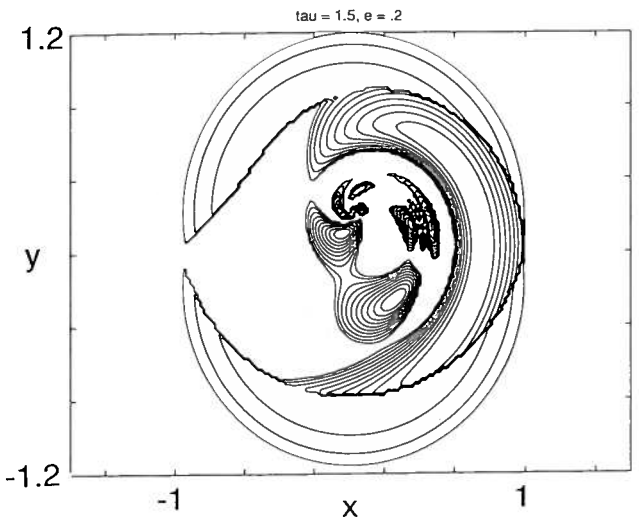

(a)

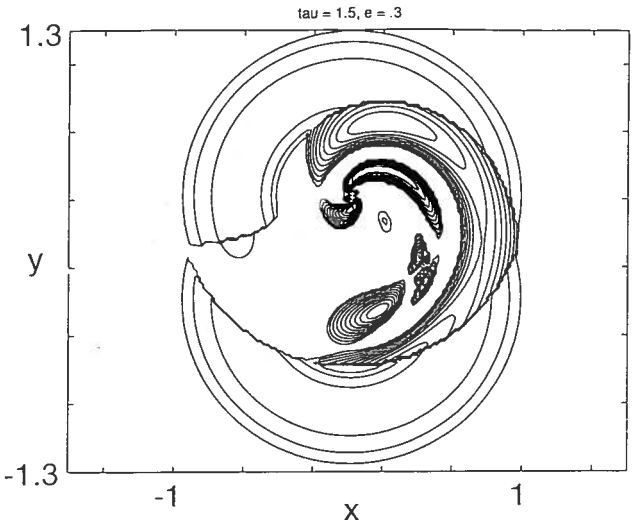

(b)

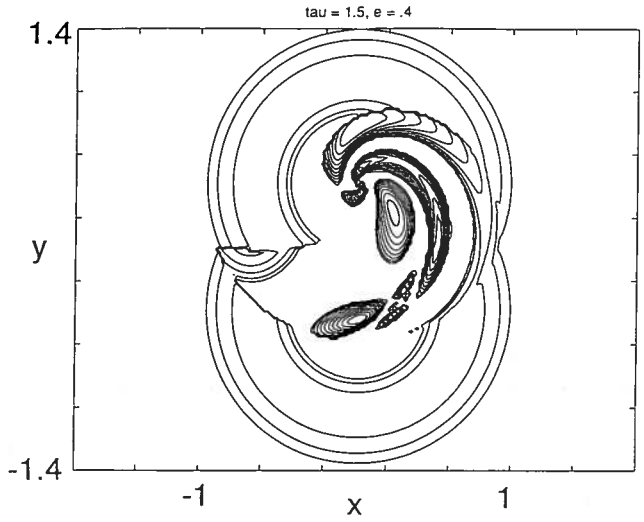

(c)

Fig. 7. The spatial variation of the maximum eigenvalue of the variational equation throughout the material for one cycle of deformation with $\tau = 1.5$ and (a) $e = 0.2$, (b) $e = 0.3$, (c) $e = 0.4$. There are ten contours ranging from 1 to 4.0 in each plot.

Then $\phi = \theta_A - \theta_B$, and

$$\mathbf{R}_\phi = \begin{bmatrix} \cos\phi & -\sin\phi \\ \sin\phi & \cos\phi \end{bmatrix} .$$

If $\mathbf{G}$ represents a full cycle of the map, then the linearization of the full cycle is $D\mathbf{G} = D\mathbf{F}|_{x_A, y_A}$ for material points which only undergo deformation during the torque about point A, and $D\mathbf{G} = D\mathbf{F}|_{x_B, y_B}$ for material points which only undergo deformation during the torque about point B. For material points which endure deformation through both half cycles, the Jacobian is

$$D\mathbf{G} = D\mathbf{F}|_{x_B, y_B} \mathbf{R}_\phi D\mathbf{F}|_{x_A, y_A} .$$

Using $D\mathbf{G}$, we can calculate the eigenvalues for any material point. Figures 6 and 7 show the spatial variation of the maximum eigenvalue of the variational map for a material point during one full cycle of deformation.

Singular values might better describe the instantaneous stretch. Either measure describes the local behavior of an infinitesimal material element, independent of its history of motion. The dynamics are not involved. This is illustrated as follows.

We consider a variational equation about a trajectory $\mathbf{z}_n$ to be a linear map of the form

$$\mathbf{u}_{n+1} = \mathbf{A}_n \mathbf{u}_n , \qquad (14)$$

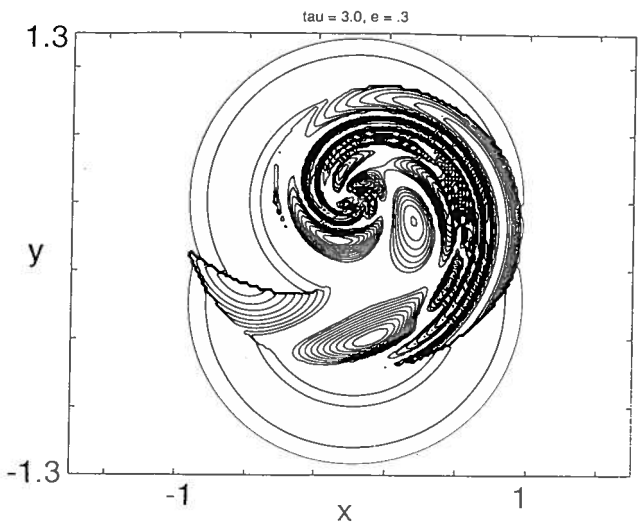

(a)

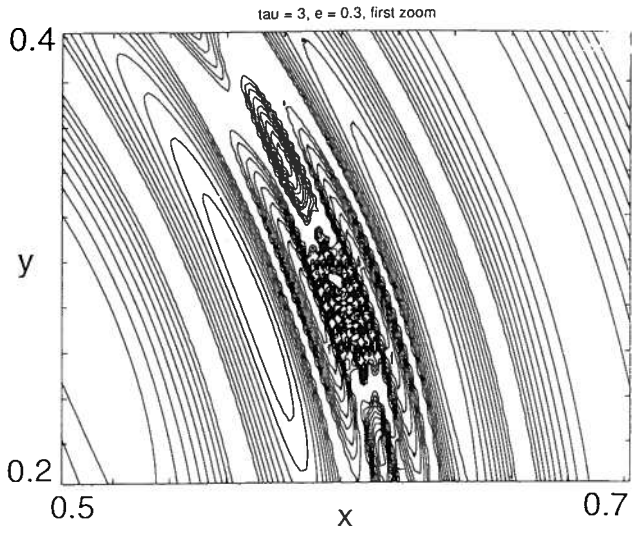

(b)

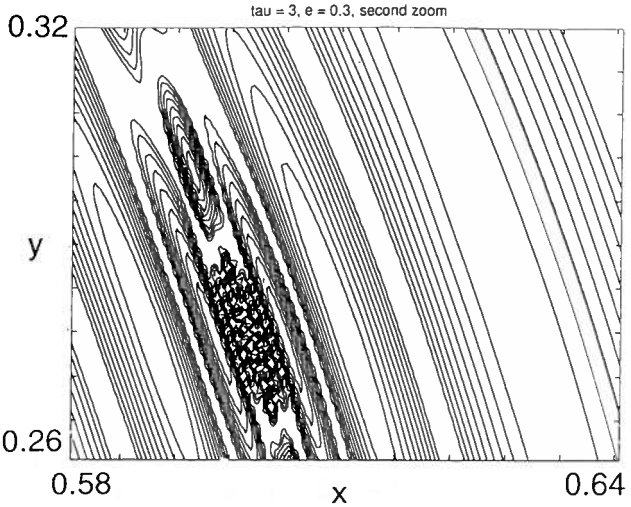

(c)

Fig. 8. There is self similarity in the spatial structure of the maximum eigenvalue of the variational equation for one cycle of deformation with $\tau = 3$ and $e = 0.3$. (a) The entire field of deformation is displayed with a resolution of 100 by 130 pixels. (b) The displayed region is $x \in [0.5, 0.7]$ and $y \in [0.2, 0.4]$. (c) The displayed region is $x \in [0.58, 0.64]$ and $y \in [0.26, 0.32]$. Further zooming reproduces the same pattern. The resolutions for (b) and (c) are both 100 by 100 pixels with ten contours spanning values from one to approximately 10.9.

where $\mathbf{A}_n = D\mathbf{G}|_{\mathbf{z}_n}$. At each iteration n, the form of $\mathbf{A}_n$ changes. For linear invariant maps, we normally put the map in Jordan form by the change of coordinates $\mathbf{u} = \mathbf{T}\mathbf{v}$, where the columns of $\mathbf{T}$ are the generalized eigenvectors of $\mathbf{A}$. For variational maps, the eigenvectors will change with n, such that $\mathbf{u}_n = \mathbf{T}_n\mathbf{v}_n$. Applying this transformation to Eq. (14) yields $\mathbf{v}_{n+1} = \mathbf{T}_{n+1}^{-1}\mathbf{A}_n\mathbf{T}_n\mathbf{v}_n$. This does not put the system into Jordan form. Hence, the eigenvalues do not represent the dynamics local to an orbit. An analogous argument applied to flows leads to a similar conclusion.

The local Lyapunov exponents measure the instantaneous expansion and contraction of an infinitesimal spheroid during iterations of the map [Nese, 1989; Eckhardt & Yao, 1993]. If, for example, the direction of expansion at a particular iterate is represented by the unit vector $\mathbf{e}_n$, then the local Lyapunov exponent would be $\lambda_n = \log ||\mathbf{A}_n\mathbf{e}_n||$. Thus, for maps, the local exponent λ_n will be less than or equal to the logarithm of the maximum local singular value. While the local Lyapunov exponent is affected by the dynamical sequence of the iterated map, the local eigenvalues omit correlation

effects of the history of motion. Local eigenvalues indicate the local behavior about material points chosen randomly at an instant in time.

With this physical interpretation in mind, we examine the maximum eigenvalue throughout the material. This provides another glimpse of the spatial structure of the system. The local Lyapunov exponents would actually be a better characterization for mixing problems [Eckhardt & Yao, 1993], but there are computational difficulties in finding $\mathbf{e}$ for each material point. Other characterizations for stretching have been performed by Muzzio *et al.* [1991] and Muzzio *et al.* [1992], the latter applying multifractals and finite-time Lyapunov exponents.

The maximum of the two magnitudes of eigenvalues for the entire deformation field can be represented by a contour plot. Figures 6 and 7 show examples of the spatial structure. Each figure has ten contours and a resolution of square pixels defined such that there are 100 pixels along the x axis.

Figure 6 shows the effect of torque duration τ. Intuitively, the maximum eigenvalue in the deformation field increases as τ increases. For $e = 0.45$, Figs. 6(a)–6(c) show the cases of $\tau = 1.5$, $\tau = 2.0$, and $\tau = 3.0$. The maximum eigenvalue magnitudes for each case are 2.6, 5.8, and 10.9, respectively. For the case of $\tau = 2.5$, the largest eigenvalue is 8.12. In some cases, the maximum local eigenvalue is larger than the square of that of the half-cycle map; this is due to the composition of shearing effects. In the middle of some of the contour plots it is easy to detect what looks like an empty sea among hilly islands. The "sea" corresponds to eigenvalues equal to, or near, one.

Figure 7 shows the effect of the eccentricity e on the e spatial distribution of the largest eigenvalue. For $\tau = 1.5$, Figs. 7(a)-7(c) represent $e = 0.2, e = 0.3$, and $e = 0.4$ The maximum eigenvalue magnitude for each case is very close to 4.0. For the cases of $e = 0.1$ and $e = 0.5$, the maximum eigenvalue magnitudes are 4.0 and 3.96.

In summary, we see the influence of parameters on the dynamically uncorrelated material behavior and on the spatial distribution of this behavior. Apparently, torque duration τ is most significant in creating large eigenvalues. Eccentricity has some effect on the spatial distribution, but very little effect on the maximum magnitudes.

The contours in Figs. 6 and 7 are congested in some areas. To obtain qualitative information, we zoom into such a region and examine the structure. We choose the case of $\tau = 3$ and $e = 0.3$ since it displays a good example of congested contours. Figure 8(a) shows the spatial distribution of maximum eigenvalues of $D\mathbf{G}$. Figure 8(b) zooms into the region defined by $x \in [0.5, 0.7]$ and $y \in [0.2, 0.4]$. The result clarifies the edges of the congested area in Fig. 8(a), but congested features remain. Figure 8(c) zooms again on this congested area, such that $x \in [0.58, 0.64]$ and $y \in [0.26, 0.32]$. Its structure is remarkably similar to that of Fig. 8(b). Zooming further reproduces the same pattern.

The area of the zoom represents material points which are mapped near the point B during the first half cycle. Thus, during the second half cycle, they experience the previously noted small-τ stretching characteristics: oscillating eigenvalues with logarithmically varying wavelengths (as τ varies). In contrast to the fractal clustering quantified by Muzzio *et al.* [1992] in a chaotic mixing flow, this self similarity is centered at a single location.

5. Conclusions

Under simplifying assumptions, the torsional deformation of a planar, rigid, perfectly plastic material slab is shown to result in a simple area-preserving logarithmic map. Application of this deformation history in a cyclic pattern, similar to the blinking vortex model, shows that complex spatial deformation patterns can result in plastic materials. The Poincaré maps show both quasiperiodic and stochastic-looking behavior, while stretching and folding of line elements presents evidence for a horseshoe mechanism in the map. The spatial distribution of eigenvalues has self-similarity in its structure. Maximum eigenvalues correlate with indications that the torque time is a key player in mixing. Application of this "chaotic mixing" of plastic materials to more practical examples is under study by the authors.

References

Acrivos, A. ed., [1991] *Physics of Fluids* **A3**(5).

Aref, H. [1984] "Stirring by chaotic advection," *Journal of Fluid Mechanics* **143**, 1–21.

Aref, H. [1986] "Chaotic advection in a Stokes flow," *Physics of Fluids* **29**(11), 3515–3521.

Chaiken, J., Chu, C. K., Tabor, M. & Tan, Q. M. [1987] "Lagrangian turbulence and spatial complexity in a Stokes flow," *Physics of Fluids* **30**(3), 687–694.

Eckhardt, B. & Yao, D. [1993] "Local Lyapunov exponents in choatic systems," *Physica* **D65**, 100–108.

Franjione, J. G., Chik-Weng Leong G.-W. & Julio M. Ottino D. M. [1989] "Symmetries within chaos: A route to effective mixing," *Physics of Fluids* **A1**(11), 1772–1783.

Ling, H. F. [1993a] "Bifurcations and mixing windows in piecewise steady mixing systems," *Process Mixing — Chemical and Biological Applications: Part II*, G. B. Tatterson, R. V. Calbrese & W. R. Penney, eds. AiChE Symposium Series 293, 55–60.

Ling, H. F. [1993b] "Chaotic mixing in a spatially periodic continuous mixer," *Physics of Fluids* **A5**(9), 2147–2160.

Mendelson, A. [1968] *Plasticity: Theory and Application* (MacMillan, New York).

Muzzio, F. J., Swanson, P. D. & Ottino, J. M. [1991] "The statistics of stretching and stirring in chaotic flows," *Physics of Fluids* **A3**(5), 822–834.

Muzzio, F. J., Meneveau, C., Swanson P. D. & Ottino, J. M. [1992] "Scaling and multifractal properties of mixing in chaotic flows," *Physics of Fluids* **A4**(7), 1439–1456.

Nese, J. M. [1989] "Quantifying local predictability in phase space," *Physica* **D35**, 237–250.

Ottino, J. M. [1989a] *The Kinematics of Mixing: Stretching, Chaos, and Transport* (Cambridge University Press, New York).

Ottino, J. M. [1989b] "The mixing of fluids," *Scientific American*, **January**, 56–67.

Ottino, J. M., Juna, S. C. & Chakravarthy, V. S. [1994] "From Reynolds's stretching and folding to mixing studies using horseshoe maps," *Physics of Fluids* **6**(2), 685–699.

Timoshenko, S. P. & Goodier, J. N. [1970] *Theory of Elasticity* (McGraw-Hill Book Company, New York).